

Attribution-NonCommercial-NoDerivatives 4.0 International (CC BY-NC-ND 4.0)

<https://creativecommons.org/licenses/by-nc-nd/4.0/>

Access to this work was provided by the University of Maryland, Baltimore County (UMBC) ScholarWorks@UMBC digital repository on the Maryland Shared Open Access (MD-SOAR) platform.

**Please provide feedback**

Please support the ScholarWorks@UMBC repository by emailing [scholarworks-group@umbc.edu](mailto:scholarworks-group@umbc.edu) and telling us what having access to this work means to you and why it's important to you. Thank you.

## Abstract

Most pathogenic bacteria require ferrous iron ( $\text{Fe}^{2+}$ ) in order to sustain infection within hosts. The ferrous iron transport (Feo) system is the most highly-conserved prokaryotic transporter of  $\text{Fe}^{2+}$ , but its mechanism remains to be fully characterized. Most Feo systems are composed of two proteins: FeoA, a soluble SH3-like accessory protein and FeoB, a membrane protein that translocates  $\text{Fe}^{2+}$  across a lipid bilayer. Some bacterial *feo* operons encode FeoC, a third soluble, winged-helix protein that remains enigmatic in function. We previously demonstrated that select FeoC proteins bind  $\text{O}_2$ -sensitive [4Fe-4S] clusters via Cys residues, leading to the proposal that some FeoCs could sense  $\text{O}_2$  to regulate  $\text{Fe}^{2+}$  transport. However, not all FeoCs conserve these Cys residues, and FeoC from the causative agent of cholera (*Vibrio cholerae*) notably lacks any Cys residues, precluding cluster binding. In this work, we determined the NMR structure of VcFeoC, which is monomeric and conserves the helix-turn-helix domain seen in other FeoCs. In contrast, however, the structure of VcFeoC reveals a truncated winged  $\beta$ -sheet in which the cluster-binding domain is notably absent. To test the interactions of VcFeoC with VcFeoB, we used NMR to demonstrate that these proteins interact in a 1:1 stoichiometry with a  $K_d$  of *ca.* 25  $\mu\text{M}$ . Finally, using homology modeling, we predicted the structure of VcNFeoB and used docking to identify an interaction site with VcFeoC, which is confirmed by NMR spectroscopy. These findings provide the first atomic-level structure of VcFeoC and contribute to a better understanding of its role vis-à-vis FeoB.

## Keywords

Feo; Ferrous iron transport protein C; ferrous iron transport protein B; nuclear magnetic resonance; helix-turn-helix; [4Fe-4S] cluster

# Introduction

Iron is essential for nearly all organisms, as it is required for indispensable cellular processes from electron transport and ATP synthesis to DNA biosynthesis [1, 2]. Given this importance, the acquisition of iron is thus necessary for the survival of nearly every organism. For many pathogenic bacteria, iron is typically obtained from a host as siderophore-bound ferric iron ( $\text{Fe}^{3+}$ ), iron protoporphyrin IX (heme), and/or ferrous iron ( $\text{Fe}^{2+}$ ), and the acquisition of this element is necessary to establish and to maintain infection [2-7]. Methods of  $\text{Fe}^{3+}$  and heme acquisition have been well-characterized, but pathways for  $\text{Fe}^{2+}$  uptake are less well-understood.

The ferrous iron transport system (Feo) is the most conserved and broadly-distributed system dedicated to  $\text{Fe}^{2+}$  transport in prokaryotes [5]; however, the precise mechanism of Feo-mediated iron transport remains unclear. The *feo* operon is generally bipartite and encodes for FeoA, a small (*ca.* 8 kDa), cytosolic SH3-like protein [8] and for FeoB, a large (*ca.* 85 kDa) transmembrane protein capable of NTP hydrolysis at its soluble N-terminal domain (typically termed NFeoB) [9]. However, in approximately 13% of bacteria the *feo* operon is tripartite and additionally encodes for FeoC, a small (*ca.* 9 kDa), cytosolic protein [10-12]. Structures of FeoC have demonstrated its architecture to include a conserved, trihelical helix-turn-helix (HTH) domain fused to a winged  $\beta$ -sheet, akin to that of the LysR transcriptional regulator (LTTR) family [10, 11, 13]. This structural similarity has led to proposals that FeoC may have a function in transcriptional regulation [14], but this hypothesis has not been verified experimentally. Additionally, sequence alignments of FeoC proteins highlight the strong conservation of Cys residues within the winged  $\beta$ -sheet, which initially suggested an iron-dependent function of FeoC that could be similar to the iron-sensing diphtheria toxin repressor (DtxR) [15, 16].

Our lab recently determined that *Escherichia coli* and *Klebsiella pneumoniae* FeoCs (*Ec* and *Kp*FeoC, respectively) bind [4Fe-4S] clusters using their Cys-rich winged  $\beta$ -sheet [16, 17]. Although the specific impact of cluster binding on iron transport is currently unknown, we demonstrated that this cluster binding event induces conformational changes in FeoC, which we posited could trigger FeoC-mediated regulation of Feo function, perhaps through interactions with FeoB at its cytosolic domain [17]. Notably, an X-ray crystal structure of the N-terminal domain of FeoB (NFeoB) from *K. pneumoniae* in complex with *Kp*FeoC has been determined (PDB ID 4AWX; [10]) but the winged  $\beta$ -sheet including its [Fe-S] cluster-binding domain was disordered, precluding assignments of protein-protein interactions of this domain. We also demonstrated that the [4Fe-4S] cluster rapidly degrades upon O<sub>2</sub> exposure, which led to the hypothesis that FeoC may regulate Feo function by sensing O<sub>2</sub> at the [Fe-S] cluster, similar to the fumarate and nitrate reductase (FNR) response regulator [17-19]. Unfortunately, this rapid reactivity in the presence of minute amounts of O<sub>2</sub> made characterizing the structure of the [4Fe-4S] cluster-bound form of FeoC difficult even under anoxic conditions. However, some FeoC proteins, including *Vibrio cholerae* FeoC (*Vc*FeoC), are required for iron transport but do not feature the Cys residues necessary for [Fe-S] cluster-binding based on sequence predictions [12, 20, 21]. Thus, we propose that *Vc*FeoC may belong to a class of FeoC proteins that do not require [Fe-S] cluster-binding and may not be iron-regulated directly but could maintain a state of constitutive activity in their interactions with FeoB [12].

To this end, we employed solution NMR spectroscopy to determine the first three-dimensional structure of *Vc*FeoC. Gel filtration and NMR data demonstrate that *Vc*FeoC is monomeric in solution under the conditions employed. Importantly, our new structure shows that *Vc*FeoC bears a HTH domain conserved among FeoCs; however, the winged  $\beta$ -sheet is shortened

and compacted relative to other FeoC proteins and does not conserve the [Fe-S] cluster-binding domain. To test whether *VcFeoC* could bind to *VcFeoB* in the absence of metal, we orthogonally cloned, expressed, solubilized, and purified intact *VcFeoB* and performed 2D NMR titration assays. These studies allowed us to approximate the binding between *VcFeoB* and *VcFeoC*, and to map *VcFeoC* residues that contribute to the binding interface. Finally, we generated a homology model of the soluble N-terminal domain of *VcFeoB* (*VcNFeoB*) and performed docking studies in an effort to identify regions of *NFeoB* involved with *VcFeoC* binding. Our findings thus reveal the first structure of *VcFeoC* and how this small protein uses its truncated winged  $\beta$ -sheet to bind to *VcFeoB*, lending further insight into the role of FeoC within the Feo system.

# Experimental methods

## Materials

The codon-optimized genes encoding *Vibrio cholerae* serotype O1 FeoC (VcFeoC; Uniprot identifier C3LP26) and *Vibrio cholerae* serotype O1 (strain M66-2) FeoB (Uniprot identifier C3LP27) were synthesized by GenScript. Materials used for buffer preparation, protein expression, and protein purification were purchased from standard commercial suppliers and were used as received. Isotopically-enriched ammonium chloride ( $^{15}\text{NH}_4\text{Cl}$ ) and glucose (globally  $^{13}\text{C}_6$ -labeled) were purchased from Cambridge Isotope Laboratories and used as received. Detergents were purchased from Sigma-Aldrich, stored at  $-20\text{ }^{\circ}\text{C}$ , and used as received.  $\text{D}_2\text{O}$  was purchased from MilliporeSigma and used as received.

## Expression and purification of VcFeoC

The cloning, expression, and purification of VcFeoC was similar to our previous FeoC preparations [17]. Briefly, DNA encoding the gene for *Vibrio cholerae* serotype O1 FeoC (VcFeoC; Uniprot identifier C3LP26) with an N-terminal  $(\text{His})_6$  tag, maltose binding protein followed by a Tobacco Etch Virus (TEV)-protease cleavage site (ENLYFQG) was sub-cloned into a pET45b(+) vector, transformed into chemically-competent BL21 (DE3) *E. coli* cells (Millipore Sigma, Burlington, MA), plated on Luria-Bertani (LB) agar plates containing  $100\text{ }\mu\text{g/mL}$  ampicillin (final concentration), and incubated at  $37\text{ }^{\circ}\text{C}$  overnight. A single colony was used to generate large-scale ( $4\times 1\text{ L}$ ) cell cultures grown in LB supplemented with  $100\text{ }\mu\text{g/mL}$  ampicillin. Cells were grown at  $37\text{ }^{\circ}\text{C}$  until reaching an  $\text{OD}_{600}$  of 0.6-0.8 at which point the cells were cold shocked briefly at  $4\text{ }^{\circ}\text{C}$ . For isotopically-enriched samples, a  $100\text{ mL}$  LB starter culture treated with  $100\text{ }\mu\text{g/mL}$  ampicillin was grown at  $30\text{ }^{\circ}\text{C}$  overnight and was used to inoculate  $4\times 1$

L of M9 minimal medium containing  $^{15}\text{NH}_4\text{Cl}$  and/or  $^{13}\text{C}_6\text{-glucose}$  (Cambridge Isotope, Tewksbury, MA, USA). The cells were grown in this isotopically-enriched minimal media at 37 °C and shaken at 200 rpm until the  $\text{OD}_{600}$  reached 0.6-0.8 before a brief cold shock at 4 °C. Both natural abundance and isotopically-enriched samples were treated with isopropyl- $\beta$ -D-1-thiogalactopyranoside (IPTG) to a final concentration of 1 mM and incubated at 18 °C with shaking at 200 rpm for 16-20 hours before harvesting by centrifugation at  $4,800 \times g$ , 10 minutes, 4 °C. Cell pellets were resuspended in resuspension buffer (50 mM Tris, pH 7.5, 200 mM NaCl, 5% v/v glycerol), treated with approximately 50-100 mg solid phenylmethylsulfonyl fluoride (PMSF), and lysed by microfluidization (Microfluidics, Westwood, MA, USA). The lysate was clarified by ultracentrifugation at  $163,000 \times g$  for 1 hour at 4 °C. The supernatant was applied to two tandem 5 mL MBPTrap HP columns (Cytiva, Marlborough, MA) and purified as previously described [17]. Fractions containing the target protein were concentrated using a 15 mL Amicon with 30 kDa molecular-weight cutoff (MWCO) spin concentrator, buffer exchanged into TEV-protease cleavage buffer (50 mM Tris, pH 8.0, 200 mM sodium chloride, 5% v/v glycerol, 1 mM TCEP, 0.5 mM ethylenediaminetetraacetic acid (EDTA)), and concentrated to 1 mL. The concentrated sample was treated with TEV protease and rocked at 4 °C overnight. The TEV-treated sample was purified by size-exclusion chromatography (SEC) using a 120 mL Superdex 75 column equilibrated with SEC buffer (25 mM Tris, pH 7.5, 100 mM sodium chloride, 5% v/v glycerol); cleaved, purified VcFeoC was concentrated using a 15 mL 3 kDa MWCO spin concentrator. This purification approach yielded *ca.* 1-3 mg VcFeoC  $\text{L}^{-1}$  of cell culture. Protein purity was assessed using 20% SDS-PAGE.

### *NMR spectroscopy of VcFeoC*

Each NMR sample contained *ca.* 2 mg of protein and was prepared in 50 mM sodium phosphate (pH 6.0), 5 mM sodium chloride with either 10% or 99% v/v D<sub>2</sub>O. Samples prepared in 99% D<sub>2</sub>O were exchanged from H<sub>2</sub>O using a PD-10 desalting column (Cytiva, Marlborough, MA). The PD-10 column was treated with 1.5 CVs of D<sub>2</sub>O, equilibrated with 1.5 CVs of NMR buffer prepared in D<sub>2</sub>O (50 mM sodium phosphate, pH 6.0, 5 mM NaCl), and eluted using 2 CVs of buffer. NMR datasets were acquired at 25 °C on a Bruker 600 MHz spectrometer equipped with a cryogenic probe. Heteronuclear single quantum coherence (HSQC) experiments were used to establish that VcFeoC was folded and served as a basis for protein backbone assignments. Standard triple resonance experiments (CBCA(CO)NH, HNCACB, HNCO, and HN(CA)CO) were collected to assign the protein backbone [22-25]. A series of two-, three-, and four-dimensional nuclear Overhauser effect spectroscopy (NOESY) data were collected for combinations of natural abundance and isotopically-labeled (<sup>15</sup>N, <sup>13</sup>C, and <sup>15</sup>N/<sup>13</sup>C) protein samples. Protein dynamics were evaluated by <sup>1</sup>H-<sup>15</sup>N heteronuclear nuclear Overhauser effect (XNOE) analysis. Data were processed with NMRPipe/nmrDraw or NMRFX and analyzed using NMRViewJ [26-29].

### *Structural calculations*

Structural calculations in torsion angle space were carried out using CYANA [30]. Upper interproton distance limits of 2.7, 3.3, and 5.0 Å were used for NOE cross-peaks of strong, medium, and weak intensities, respectively. Appropriate corrections of interproton distance limits were made for pseudoatoms. The TALOS+ Server was used to determine dihedral restraints that were incorporated into structural calculations based on amide proton, amide nitrogen, H $\alpha$ , C $\alpha$ , C $\beta$ , and carbonyl carbon chemical shifts [31]. PyMOL was employed to

prepare structural figures [32]. The atomic coordinates for VcFeoC were deposited in the RCSB database (PDB ID 7U37). NMR chemical shifts and corresponding structure refinement parameters were deposited in the BMRB database (BMRB accession number 30995).

### *Expression and purification of VcFeoB*

The gene encoding for the *Vibrio cholerae* serotype O1 (strain M66-2) FeoB protein (Uniprot identifier C3LP27) was engineered to contain a C-terminal TEV-protease cleavage site (ENLYFQS) followed by a (His)<sub>6</sub> tag for affinity chromatography purification and subcloned into the pET-21a(+) expression plasmid. This plasmid was transformed into chemically-competent BL21 (DE3) *E. coli* expression cells similar to the MBP-VcFeoC construct. Large-scale expression of the protein was accomplished in 12 baffled flasks charged with 1 L of modified Terrific Broth supplemented with 100 µg/mL ampicillin. Growth was carried out at 37 °C with shaking at 200 rpm and monitored until an OD<sub>600</sub> of 1.5-1.75 was reached. Flasks containing cells and media were then cold-shocked for at 4 °C before inducing protein expression with the addition of IPTG to a final concentration of 1 mM. Protein expression was carried out at 18 °C with shaking of 200 rpm overnight. After 18-20 h, the cells were harvested by centrifugation at 4800 ×g, 12 min, 4 °C. Cell pellets were resuspended in resuspension buffer (25 mM Tris, pH 7.5, 100 mM sucrose) and flash-frozen in N<sub>2</sub> (l) before storage at -80 °C.

All purifications of VcFeoB were carried out at 4 °C unless otherwise noted. Briefly, frozen cells containing the expressed protein were thawed and supplemented with solid PMSF (approximately 50-100 mg) before being lysed using a Q700 ultrasonic cell disruptor (QSonica, Newtown, CT) operating at 80% maximal amplitude, 30 s pulse on, 30 s pulse off, for a total duration of 12 min total pulse-on time. The lysate was then spun at 10000 ×g for 1 h to separate

cellular debris and suspended membranes. The supernatant was decanted and ultracentrifuged at  $163000 \times g$  for 1 h. Pelleted membranes were then washed, resuspended, and rehomogenized in resuspension buffer. Protein concentration was measured using the detergent-compatible (DC) Lowry assay (Bio-Rad Laboratories, Hercules, CA) before being flash-frozen on  $N_2$  (*l*) and stored at  $-80^\circ C$ . Membranes containing the VcFeoB protein were thawed and solubilized with vigorous stirring for 3 h at  $4^\circ C$  by the addition of a 10% (w/v) stock n-dodecyl- $\beta$ -D-maltopyranoside (DDM) to a final concentration of 1% (w/v) detergent and 3-5 mg/mL total protein concentration. Insoluble material was then pelleted by ultracentrifugation at  $163,000 \times g$  for 1 h before applying the supernatant to a 5 mL HisTrap HP column (Cytiva, Marlborough, MA) charged with  $Ni^{2+}$  and equilibrated with 10 column volumes (CVs) of wash buffer (25 mM Tris, pH 8, 100 mM sucrose, 300 mM NaCl, 1mM TCEP and 0.05 % (w/v) DDM) containing 21 mM of imidazole. After application of the clarified lysate, the column was then washed with 10 CVs of wash buffer containing 21 mM of imidazole. The protein was eluted by the wash buffer containing 150 mM imidazole. Fractions containing VcFeoB were concentrated with a 15 mL Amicon 100 kDa MWCO spin concentrator (Millipore Sigma, Burlington, MA) and buffer exchanged into wash buffer using a PD-10 desalting column (Cytiva, Marlborough, MA). Protein purity was assessed via 15% SDS-PAGE analysis. Through this purification method, *ca.* 3-5 mg of pure VcFeoB was obtained  $L^{-1}$  of cultured cells.

#### *Titration of VcFeoB into VcFeoC*

Purified VcFeoB and VcFeoC samples were buffer exchanged into the VcFeoB wash buffer (25 mM Tris, pH 8, 100 mM sucrose, 300 mM NaCl, 1mM TCEP and 0.05 % (w/v) DDM). HSQC spectra were collected as VcFeoB was titrated into 100  $\mu M$  VcFeoC samples at

stoichiometric (mole:mole) ratios of 0:1, 0.25:1, 0.5:1, and 1:1. Protein precipitation was observed at stoichiometric ratios greater than 1:1, preventing acquisition of further titration datapoints. The dissociation constant ( $K_d$ ) was estimated by integrating 1D  $^1\text{H}$  NMR spectra over the region in which VcFeoC amide signals were detected (6.5-9.5 ppm) for all titration points. The fraction of VcFeoB bound to VcFeoC was determined by calculating the ratio of free VcFeoC signal after VcFeoB titration relative to unbound VcFeoC, and these data were used to generate a binding isotherm. Data were processed using NMRFX [27], data integrations were carried out using dataChord Spectrum Analyst (One Moon Scientific, Inc., Westfield, NJ), and the binding isotherm fit was determined using Igor Pro (Wavemetrics, Lake Oswego, OR).

#### *Predicted docking model of VcNFeoB and VcFeoC*

A homology model of VcNFeoB was predicted by using ColabFold [33], which applies the AlphaFold2 structural prediction approach using MMseqs2 and HHSearch [34]. Docking studies were carried out for the lowest-energy predicted model in combination with the NMR structure of VcFeoC by utilizing the ClusPro online server without modification to the default settings and restraints [35, 36]. The selected docking model chosen was that with the lowest balanced, weighted score that was also consistent with the NMR titration data.

## Results

### *Expression, purification, cleavage, and isolation of VcFeoC*

The expression, purification, cleavage, and isolation of untagged VcFeoC from the MBP-tagged construct was carried out similarly to previously described approaches for *E. coli* and *K. pneumoniae* FeoC proteins (*EcFeoC* and *KpFeoC*, respectively) (Fig. S1) [17]. Specific deviations from the earlier reported methods included: (1) isolation of VcFeoC from the tagged protein by carrying out the Tobacco Etch Virus (TEV)-protease cleavage reaction at 4 °C instead of room temperature to maintain solubility and (2) purification in the absence of reducing agent given that VcFeoC lacks redox-sensitive Cys residues unlike *Ec* and *KpFeoC*. This approach gave rise to yields of *ca.* 1-3 mg of highly pure protein L<sup>-1</sup> of cell culture (Fig. S1). Notably, some reports suggest that the Feo system is only operative in an oligomerized, trimeric form; however, we see no evidence for formation of trimeric VcFeoC, which behaves as a monomeric protein in solution based on data from gel filtration experiments (Fig. S1) and NMR analyses (*vide infra*). These results are consistent with previous results from our lab on NFeoAB (a fusion between FeoA and NFeoB), FeoA, and FeoC, which all appear as predominately monomeric species in our hands [17, 37, 38].

### *Secondary structure of VcFeoC*

Due to the small nature and good accumulation of recombinant VcFeoC, nuclear magnetic resonance (NMR) spectroscopy was employed for structural and dynamics analyses. Gel filtration profiles under NMR conditions indicated that VcFeoC was monodisperse and monomeric (Fig. S1B), consistent with previous findings reported for FeoC proteins [11, 17]. High-quality 2D <sup>1</sup>H-<sup>15</sup>N heteronuclear single quantum coherence (HSQC) spectra were acquired

for purified *VcFeoC* (Fig. 1A), which demonstrated well-dispersed amide signals indicative of folded protein [39]. Although the  $^1\text{H}$  and  $^{15}\text{N}$  chemical shifts were generally insensitive to protein concentration (100-700  $\mu\text{M}$ ) and sample pH (6.0-8.0) (data not shown), backbone amide assignments were made at pH 6.0 due to optimal long-term protein stability and a decreased  $^1\text{H}$ -

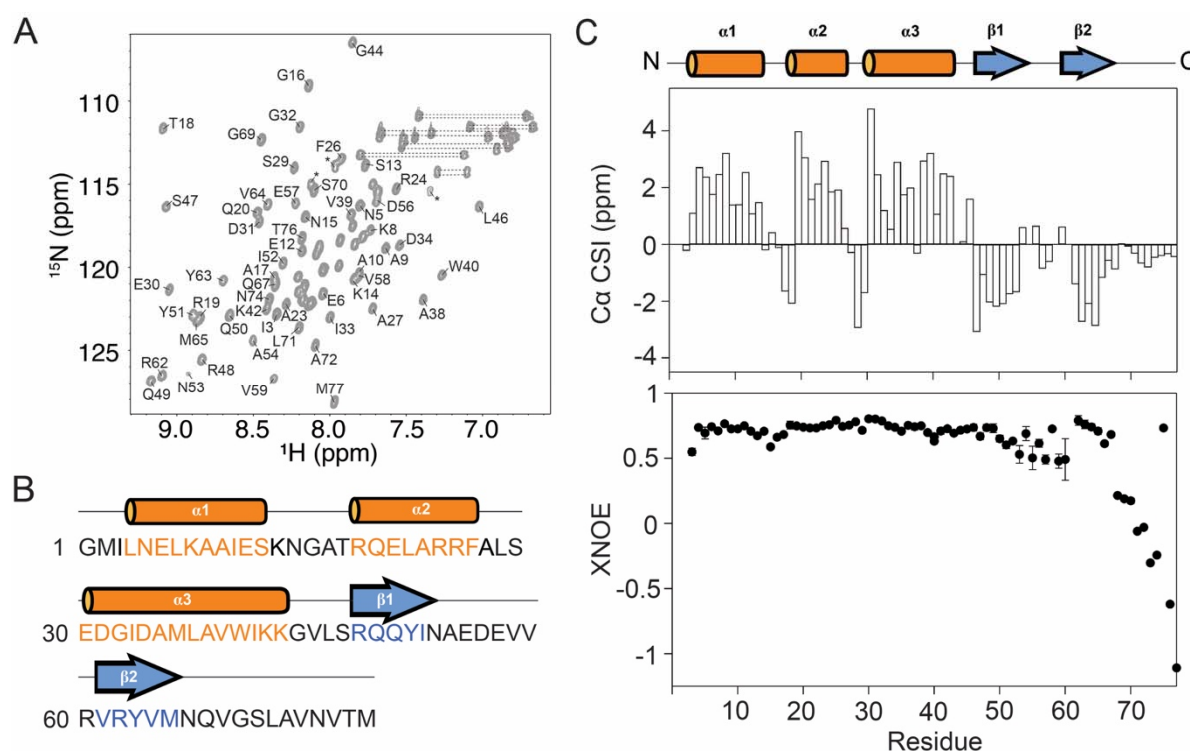


**Figure 1.** The secondary structure determination of *VcFeoC*. **A.** Assigned  $^1\text{H}$ - $^{15}\text{N}$  HSQC NMR spectrum of 300  $\mu\text{M}$  *VcFeoC* at 298 K (50 mM sodium phosphate, pH 6.0, 5 mM NaCl, 10% v/v  $\text{D}_2\text{O}$ ). Assignments are generally explicit for residues in the less-crowded regions. Dashed lines represent signals corresponding to Asn and Gln side chains. Asterisks represent signals from Arg side chains. **B.** Amino acid sequence of *VcFeoC* mapped with a cartoon of the corresponding secondary structure of each region. Residues belonging to  $\alpha$ -helices are highlighted in orange ( $\alpha$  labels) and include the following regions: Leu<sup>4</sup> to Ser<sup>13</sup> ( $\alpha$ 1), Arg<sup>19</sup> to Phe<sup>26</sup> ( $\alpha$ 2), and Glu<sup>30</sup> to Lys<sup>42</sup> ( $\alpha$ 3). The two-stranded  $\beta$ -sheet ( $\beta$  labels; blue) is composed of residues Arg<sup>48</sup> to Ile<sup>52</sup> ( $\beta$ 1) and Val<sup>61</sup> to Met<sup>65</sup> ( $\beta$ 2). Note: a single additional Gly residue at the N-terminus is present as a result of the TEV cleavage reaction. **C.** NMR chemical shift indices for backbone  $\text{C}\alpha$  atoms of *VcFeoC* (top panel); positive values represent  $\alpha$ -helical regions, negative stretches represent  $\beta$ -strand residues, and near zero values indicate unstructured and/or random coil regions.  $^1\text{H}$ - $^{15}\text{N}$  heteronuclear NOE (XNOE) data (bottom panel) indicate that *VcFeoC* is largely structured with the exception of dynamic linkers (Lys<sup>14</sup> to Thr<sup>18</sup>, Arg<sup>25</sup> to Ser<sup>29</sup>, and Lys<sup>43</sup> to Ser<sup>47</sup>), the dynamic wing region (Asn<sup>53</sup> to Arg<sup>60</sup>), and the C-terminal tail (Asn<sup>66</sup> to Met<sup>77</sup>). The amide signal of Val<sup>5</sup> is overlaid with that of Glu<sup>21</sup> ( $\alpha$ 2) and therefore gives an XNOE more consistent with a structured element. Error bars represent the standard

$^2\text{H}$  exchange of amide protons [40]. The established NMR conditions allowed for assignment of all backbone amide signals except for that of Val 61 (99% completion).

To determine the secondary structure of VcFeoC, the  $\text{C}\alpha$  chemical shift indices (CSI) were analyzed based on assignment of triple resonance spectra (Fig. 1B-C) [41]. This analysis indicated that VcFeoC is composed of three  $\alpha$ -helices ( $\alpha 1$ , Leu<sup>4</sup> to Ser<sup>13</sup>;  $\alpha 2$ , Arg<sup>19</sup> to Phe<sup>26</sup>;  $\alpha 3$ , Glu<sup>30</sup> to Lys<sup>42</sup>) and two  $\beta$ -strands ( $\beta 1$ , Arg<sup>48</sup> to Ile<sup>52</sup>;  $\beta 2$ , Val<sup>61</sup> to Met<sup>65</sup>), the latter of which are linked to form a short winged  $\beta$  hairpin terminating at an unstructured, dynamic C-terminal tail. Interestingly, negative  $\text{C}\alpha$  CSI values at residues immediately preceding the start of  $\alpha 2$  (Thr<sup>18</sup>) and the start of  $\alpha 3$  (Ser<sup>29</sup>) indicated the presence of N-terminal  $\alpha$ -helix capping [42, 43], a structural feature that has been shown to impart additional stability to helices [44]. To characterize further the architecture of VcFeoC, heteronuclear  $^1\text{H}$ - $^{15}\text{N}$  NOE (XNOE) data (Fig. 1C, bottom) were acquired. These data offered insight into the backbone dynamics and internal mobility for each signal, where XNOE measurements below *ca.* 0.8 are indicative of flexibility [45]. The XNOE analysis shows that VcFeoC is largely structured except for three short linkers (Lys<sup>14</sup> to Thr<sup>18</sup>, Arg<sup>25</sup> to Ser<sup>29</sup>, and Lys<sup>43</sup> to Ser<sup>47</sup>), the  $\beta$  hairpin wing residues (Asn<sup>53</sup> to Arg<sup>60</sup>), and the C-terminus (Asn<sup>66</sup> to Met<sup>77</sup>). Taken together, the XNOE findings both agree with the secondary structure determined from the  $\text{C}\alpha$  CSI data and are in general agreement with the structural architecture of previously studied FeoC proteins.

### *Tertiary structure of VcFeoC*

In order to determine the tertiary structure of VcFeoC,  $^{15}\text{N}$ - and  $^{15}\text{N}/^{13}\text{C}$ -isotopically enriched VcFeoC samples were prepared, and 3D  $^{15}\text{N}$ -edited nuclear Overhauser effect (NOE), 4D  $^{15}\text{N}/^{13}\text{C}$ -, and  $^{13}\text{C}/^{13}\text{C}$ -edited NOE NMR spectra were acquired [46-49]. After data

acquisition, structural calculations were carried out using a total of 648 interproton distance restraints derived from NOE data, 128 hydrogen bond restraints determined based on NOE cross-peak patterns, and 86 dihedral restraints based on backbone chemical shifts (Table 1). An ensemble of 20 refined structures with the lowest target function of  $0.005 \pm 0.002 \text{ \AA}^2$  was generated for VcFeoC, and this ensemble exhibited good convergence based on root-mean-square deviations (RMSDs) of  $0.12 \pm 0.04 \text{ \AA}^2$  for backbone heavy atoms (Fig. 2; Table 1).

As anticipated, the tertiary structure of VcFeoC adopts a winged helix-turn-helix (HTH) structure featuring a three-helix bundle and a two-stranded antiparallel  $\beta$ -sheet that is connected

**Table 1.** Structural restraints and refinement statistics for VcFeoC.

| NMR-derived restraints         |                                     |
|--------------------------------|-------------------------------------|
| Intraresidue                   | 319                                 |
| Sequential ( $ i-j  = 1$ )     | 216                                 |
| Hydrogen bonds                 | 113                                 |
| Dihedral angle restraints      | 86                                  |
| Total restraints               | 862                                 |
| Average restraints per residue | 11.3                                |
| Residual restraint violations  |                                     |
| CYANA target function          | $0.00526 \pm 0.00189 \text{ \AA}^2$ |
| Maximum violations             |                                     |
| Upper limits                   | $0.0021 \pm 0.0006 \text{ \AA}^2$   |
| Lower limits                   | $0.0002 \pm 0.00004 \text{ \AA}^2$  |
| Van der Waals                  | $0.04 \pm 0.01 \text{ \AA}^2$       |
| Torsion angles                 | $0.0189 \pm 0.0065 \text{ radian}$  |
| Structure convergence          |                                     |
| Pairwise rms deviations        |                                     |
| Backbone heavy atoms           | $0.12 \pm 0.04 \text{ \AA}$         |
| All heavy atoms                | $1.12 \pm 0.18 \text{ \AA}$         |
| Ramachandran analysis          |                                     |
| Most favored regions           | 91.55 %                             |
| Additional allowed regions     | 5.63 %                              |
| Generously allowed regions     | 2.82 %                              |

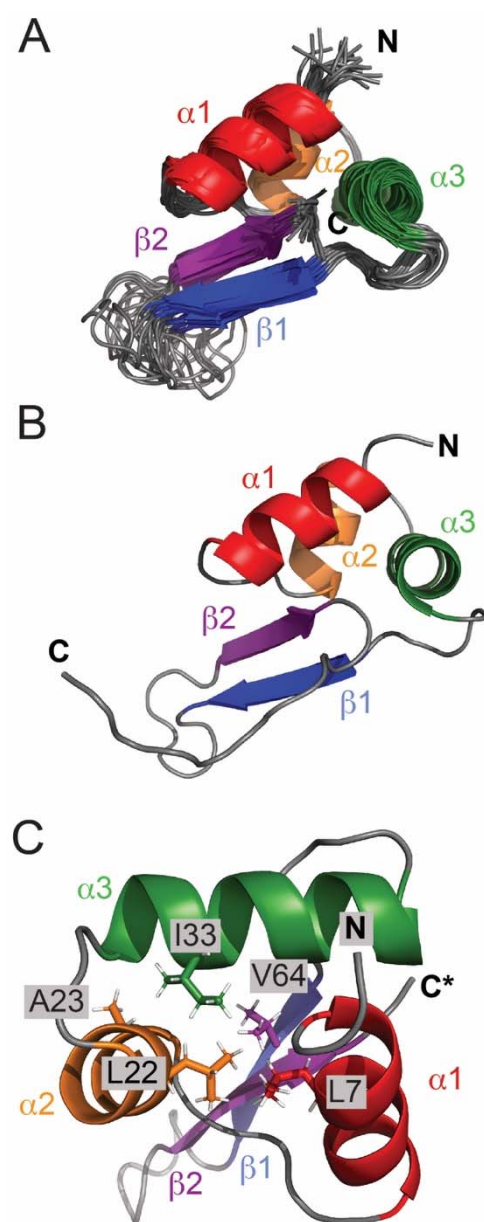


**Figure 2.** The NMR structure of VcFeoC. **A.** Superposition of the 20 lowest-energy refined structures of VcFeoC. The structured regions are Leu<sup>4</sup> to Ser<sup>13</sup> ( $\alpha 1$ ; red), Arg<sup>19</sup> to Phe<sup>26</sup> ( $\alpha 2$ ; orange), Glu<sup>30</sup> to Lys<sup>42</sup> ( $\alpha 3$ ; green), Arg<sup>48</sup> to Ile<sup>52</sup> ( $\beta 1$ ; blue), and Val<sup>61</sup> to Met<sup>65</sup> ( $\beta 2$ ; purple). The ribbon representations include Gly 1 through Gln 67 to demonstrate the globular portion of the structure, but the dynamic C-terminal tail is truncated for clarity (represented by C\*). **B.** Ribbon diagram of the full-length, lowest-energy target function structure of VcFeoC. **C.** The hydrophobic core of VcFeoC includes residues Leu<sup>7</sup>, Leu<sup>22</sup>, Ala<sup>23</sup>, Ile<sup>33</sup>, and Val<sup>64</sup>, which combined hold together the helix-turn-helix motif. The N- and C-termini are represented by 'N' and 'C' labels, respectively. Images in which the dynamic, unstructured C-terminus is truncated for figure clarity are labeled with 'C\*'.

by an unstructured wing. Long-range NOEs indicate that the hydrophobic core of *VcFeoC* is composed of residues from  $\alpha$ 1-3 (Leu<sup>7</sup>, Leu<sup>22</sup>, Ala<sup>23</sup>, and Ile<sup>33</sup>) and  $\beta$ 2 (Val<sup>64</sup>) (Fig. 2B-C). In order to quantify the similarity among *VcFeoC* and other structurally characterized FeoCs, C $\alpha$  RMSDs were determined of the following: *KpFeoC* isolated from the X-ray crystal structure of *KpFeoC* complexed with the N-terminal domain of *KpFeoB* (*KpNFeoB*) (1.793 Å; 29 C $\alpha$ s) [10], apo *KpFeoC* (1.770 Å; 22 C $\alpha$ s) [11], and *EcFeoC* (1.595 Å; 30 C $\alpha$ s) (Table 2). Superpositioning of *VcFeoC* upon these FeoC homologs highlights the similarity of the gross tertiary structure and, particularly, the conserved HTH domain (Fig. 3). Notably, the main structural differences among

FeoCs are variations in the length of the  $\beta$ -strands, the extent of the  $\beta$ -sheet length, and the diversity in the length of the unstructured wing. Intriguingly, whereas both *Ec* and *KpFeoC* have long, Cys-rich wings that serve to bind [4Fe-4S] clusters under anoxic conditions [16, 17], *VcFeoC* features a shorter wing lacking Cys residues that cannot bind an [Fe-S] cluster. Despite this change, the wing of *VcFeoC* is still quite dynamic, although it is incapable of sampling as much three-dimensional space as *Ec*- or *KpFeoC* wings, due to the size differences. It is possible that this shorter wing region of *VcFeoC* may be more constrained in space and may actually mimic the cluster-bound forms of *Ec/KpFeoC*, which are known to be more compact [17].

**Table 2.** C $\alpha$  RMSD s of the NMR-derived structure of *VcFeoC* and other bacterial FeoC structures.

| Protein                                        | PDB ID | RMSD (Å) <sup>a</sup> |
|------------------------------------------------|--------|-----------------------|
| <i>Escherichia coli</i> FeoC                   | 1XN7   | 1.595                 |
| <i>Klebsiella pneumoniae</i> FeoC              | 2K02   | 1.770                 |
| <i>Klebsiella pneumoniae</i> FeoC (FeoB-bound) | 4AWX   | 1.793                 |

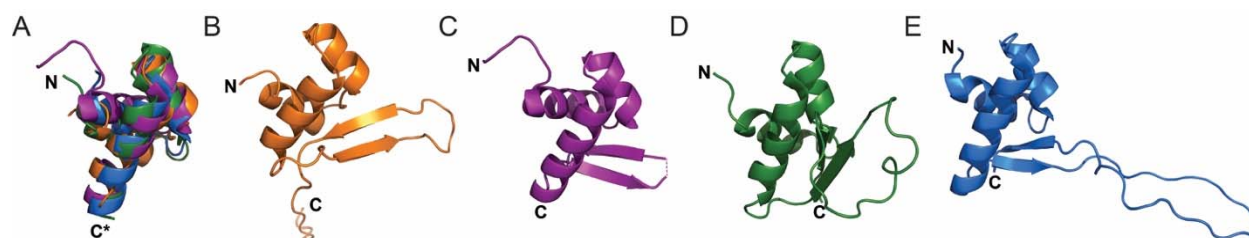


**Figure 3.** Comparisons of structurally-characterized FeoC proteins. **A.** Overlaid, truncated structures (residues 1-45) of the NMR-derived VcFeoC (orange; PDB ID 7U37), the crystal structure of *Klebsiella pneumoniae* FeoC (KpFeoC) isolated from the KpFeoC-KpNFeoB complex (purple; PDB ID 4AWX), apo KpFeoC (green; PDB ID 2K02), and *Escherichia coli* FeoC (EcFeoC, blue; PDB ID 1XN7). The superpositioning of these structures demonstrates the similarity within the conserved three-helix bundle (approximately residues 1-45 of each protein). **B-E.** Ribbon diagrams of the full-length NMR structure of VcFeoC (**B**), crystallized KpFeoC bound to NFeoB (**C**), the NMR structure of apo KpFeoC (**D**), and the NMR structure of apo EcFeoC (**E**). These comparisons illustrate the heterogeneity observed within the winged regions of the winged-helix motif among FeoC proteins. The N- and C-termini are represented by ‘N’ and ‘C’ labels, respectively. Images in which the C-terminus is truncated for figure clarity are labeled with ‘C\*’.

<sup>a</sup> Root-mean-square deviation calculated between Cα atoms of matched residues

### Interactions between VcFeoB and VcFeoC

Previous work by Hung and coworkers demonstrated the formation of a tight complex between KpFeoC and the guanine dissociation inhibitor (GDI) domain of KpNFeoB, suggesting a role for FeoC in the direct regulation of Fe<sup>2+</sup> transport [10]. However, these studies were carried out with apo KpFeoC, and the dynamic wing region was unresolved in the electron density; whether the cluster-bound form were capable of binding to KpNFeoB was not explored. Moreover, these studies were unfortunately limited in that KpFeoC was only tested for interactions with the soluble N-terminal domain of FeoB, not the intact membrane protein. In contrast, bacterial adenylate cyclase two-hybrid (BACTH) assays conducted by Weaver *et al.* indicated interaction of intact, full-length VcFeoB and VcFeoC under *in vivo* conditions [12]. Variant studies suggested that the interactions occurred between the N-terminal region of

VcFeoB and residues Glu<sup>29</sup> and Met<sup>35</sup> of VcFeoC [12], but a direct observation of these interactions had not been determined.

Thus, we sought next to determine whether VcFeoC binds to full-length VcFeoB *in vitro* and, if so, to identify the binding interface of VcFeoB-VcFeoC, which could inform previous *in vivo* immunoprecipitation findings [20]. However, probing these interactions *in vitro* required the nontrivial preparation of large amounts of full-length VcFeoB. After multiple optimization attempts, suitable heterologous expression of VcFeoB featuring a C-terminal (His)<sub>6</sub> tag was achieved. Solubilization in n-dodecyl-β-D-maltoside (DDM) and subsequent purification reproducibly resulted in the isolation of 2-3 mg of highly pure VcFeoB L<sup>-1</sup> of cells culture (Fig.

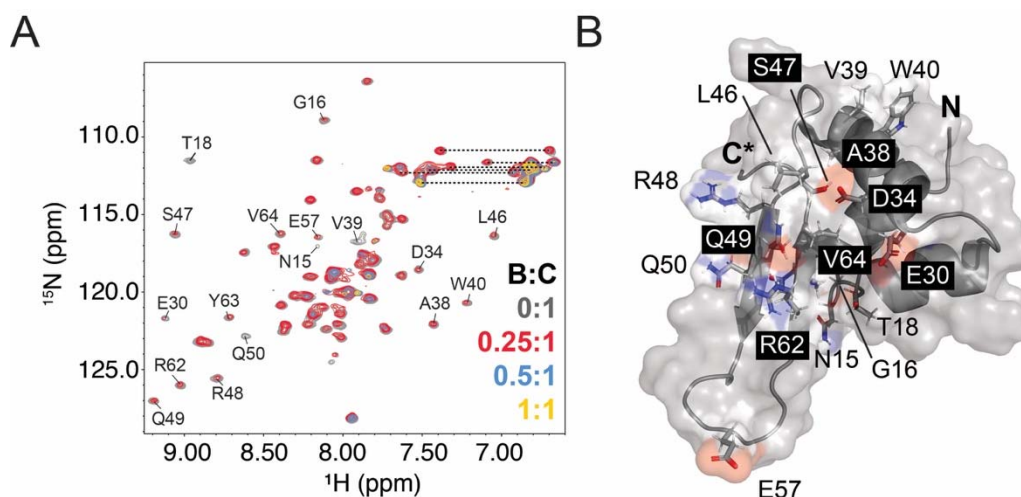


**Figure 4.** VcFeoC binds to intact VcFeoB in a 1:1 complex. **A.** Overlaid <sup>1</sup>H-<sup>15</sup>N HSQC spectra of VcFeoB titrated into 100 μM VcFeoC (gray) at stoichiometric ratios (mole:mole) of 0.25:1 (red), 0.5:1 (blue), and 1:1 (yellow) at 298 K (50 mM Tris, pH 8.0, 100 mM sucrose, 200 mM NaCl, 0.05% dodecyl-β-D-maltoside, 1 mM TCEP). VcFeoB (*ca.* 80 kDa) exceeds the limit of detection by NMR, and the broadened loss of VcFeoC signals represents formation of the VcFeoB-VcFeoC complex. Labels are included and correspond to VcFeoC signals that broaden the most rapidly due binding at the VcFeoB/VcFeoC interface. Dashed lines represent Asn and Gln side chain signals. **B.** A surface and cartoon representation of the truncated, lowest-energy structure of VcFeoC (residues 1-67) indicating that residues within the helix-turn-helix (HTH) region (Asn<sup>15</sup>, Gly<sup>16</sup>, and Thr<sup>18</sup>), linker 2 (Glu<sup>30</sup>), α3 (Asp<sup>34</sup>, Ala<sup>38</sup>-Trp<sup>40</sup>), linker 3 (Leu<sup>46</sup> and Ser<sup>47</sup>), β-sheet (Arg<sup>48</sup>-Gln<sup>50</sup>, Arg<sup>62</sup>-Val<sup>64</sup>), and wing (Glu<sup>57</sup>) broaden rapidly due to interaction with VcFeoB. Labels are included for all residues for which broadened signals are observed except for Tyr<sup>63</sup> that is on the opposite face of β2. The N- and truncated C-terminus is represented by 'N' and 'C\*' labels, respectively.

S2). To determine whether VcFeoC interacts with the intact VcFeoB *in vitro*, 2D  $^1\text{H}$ - $^{15}\text{N}$  HSQC NMR spectra of VcFeoC were acquired as VcFeoB was titrated into various stoichiometric ratios (mole:mole) of VcFeoC (Fig. 4). Given that the large size of VcFeoB (*ca.* 85 kDa) exceeds the limit of detection of NMR, formation of the VcFeoB-FeoC complex (*ca.* 94 kDa) results in a broadened and decreased NMR signal of the observed (unbound) VcFeoC (*ca.* 9 kDa). Importantly, a control detergent-to-VcFeoC titration was also performed to ensure that the decreased VcFeoC signal intensity was the result of binding to VcFeoB and not adventitious interactions with DDM micelles (Fig. S3). The overlaid HSQC data indicate that VcFeoC binds VcFeoB using the following regions on VcFeoC: Asn<sup>15</sup>, Gly<sup>16</sup>, and Thr<sup>18</sup> of the HTH domain; Glu<sup>30</sup> of linker 2 (analogous to Glu<sup>29</sup> identified in the previous BACTH studies [12]); Asp<sup>34</sup> and Ala<sup>38</sup> to Trp<sup>40</sup> of  $\alpha$ 3; Leu<sup>46</sup> and Ser<sup>47</sup> of linker 3; Arg<sup>48</sup> to Gln<sup>50</sup> and Arg<sup>62</sup> to Val<sup>64</sup>  $\beta$ -sheet; and Glu<sup>57</sup> of the wing (Fig. 4). We failed to observe any sign of interactions with the analogous Met<sup>35</sup> in the previous BACTH studies. Attempts to titrate VcFeoB into VcFeoC beyond a 1:1 (mole:mole) ratio resulted in sample precipitation; however, the existing data still facilitated estimation of the binding affinity for complex formation. To do so, the 1D  $^1\text{H}$  signal over the amide region (6.5-9.5 ppm) was integrated, the fraction of VcFeoC bound to VcFeoB was determined for each titration point, and the binding isotherm for complex formation was evaluated (Fig. S4) [50, 51]. Using this analysis, we approximate that VcFeoC binds to VcFeoB with a modest  $K_d$  of *ca.* 25  $\mu\text{M}$ , much weaker than the truncated apo *KpFeoC/KpNFeoB* complex.

As we presumed that VcFeoC interacts with the N-terminal domain of VcFeoB (VcNFeoB) based on previous data [10], but our NMR titrations only give us a spectroscopic and structural handle for VcFeoC, we then sought to understand the interaction between VcFeoC and

VcNFeoB better through modeling approaches. As several structures of NFeoB homologs exist in the PDB, we determined a homology model of VcNFeoB, and we used the lowest-energy model to dock VcFeoC onto VcNFeoB. Several docking models predicted interactions in a similar orientation to those shown in Fig. 5A, which demonstrates that electrostatic and hydrophobic interactions reinforce binding between Switch I/Switch II and the GDI domains of VcNFeoB with the winged  $\beta$ -sheet of VcFeoC, consistent with our NMR findings (*vide supra*).

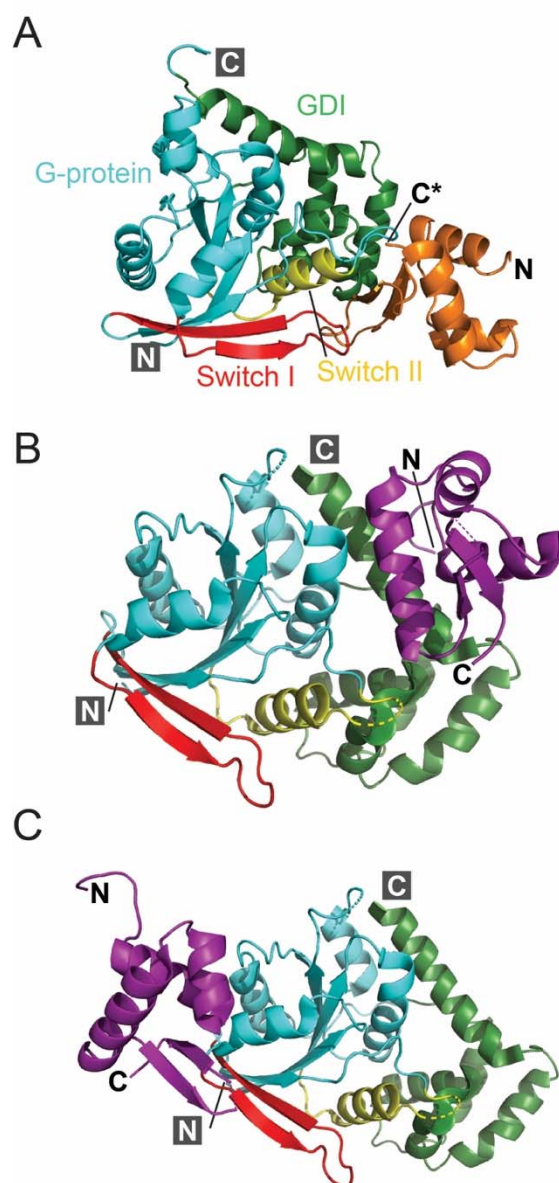


**Figure 5.** *VcFeoC-VcNFeoB* docking model and its comparison to the *KpFeoC-KpNFeoB* co-crystal structure. **A.** Docking studies of *VcFeoC* (orange) and the homology model of *VcNFeoB* suggest interactions of the *VcFeoC*  $\beta$ -sheet and wing with Switch I (red), Switch II (yellow), and GDI (green) domains. **B.** Studies of *KpFeoC* (purple) co-crystallized with *KpNFeoB* (PDB ID 4AWX) indicate that *KpFeoC*  $\alpha 3$  interacts with *NFeoB* by means of hydrogen bonds, salt bridges, and hydrophobic interactions with the GDI (green) and Switch II (yellow) domains [10]. **C.** Extended crystal contacts throughout the crystalline lattice indicate an alternative mode of binding of *KpFeoC* (purple) to *KpNFeoB* in which the *KpFeoC* wing interacts with the Switch I region of *KpNFeoB* (red). Images in which the dynamic, unstructured C-terminus is truncated for figure clarity are labeled with 'C\*'. The G-protein domain is colored in cyan. The N- and C-termini are represented by 'N' and 'C' labels, respectively.

These results are similar to those observed in the *Kp*NFeoB/*Kp*FeoC complex X-ray crystal structure (PDB ID 4AWX; Fig 5B,C). Unfortunately, in that structure the asymmetric unit (ASU) of this complex was ambiguous and suggested that *Kp*FeoC could interact with *Kp*NFeoB via hydrogen bonding, electrostatic interactions, and interactions of hydrophobic residues between two different regions: the GDI domain on a single *Kp*NFeoB protomer and the Switch II region of the neighboring *Kp*NFeoB protomer (Fig. 5B) [10]. Our modeling data suggest that both could be operative, at least for *Vc*FeoC, which may represent a constitutive mimic of the holo, [Fe-S] cluster-bound form of FeoC, which was absent from the *K. pneumoniae* complex structure.

## Discussion

Although the function of FeoC remains disputed, it is clear that this poorly conserved protein serves a regulatory function that is important for  $\text{Fe}^{2+}$  transport in several  $\gamma$ -proteobacteria [12, 21, 52]. Many of these organisms are pathogenic prokaryotes, including notable problematic pathogens such as *Salmonella enterica* [52, 53], *V. cholerae* [12], and *K. pneumoniae* [10]. Our lab has demonstrated that the role of some FeoCs is likely dependent on the binding of an oxygen-sensitive [Fe-S] cluster binding in the dynamic wing regions of FeoC [17], contrasting earlier studies suggesting that these cluster-binding FeoCs could be oxygen-tolerant [16]. Studies of *S. enterica* FeoC further confirm that FeoC is oxygen-sensitive and could regulate FeoB levels under changing metabolic conditions [53]. Unfortunately, the oxygen-sensitive nature of the [Fe-S] cluster makes structural determination of cluster-replete FeoCs challenging [17]. However, some FeoC proteins in pathogens like *V. cholerae* lack the necessary cluster-binding residues, prohibiting [Fe-S] cluster binding, yet these proteins remain functionally important [12, 17, 20]. These observations have led us to hypothesize that the functional aspect of FeoC may either be located at a structural site outside of the [Fe-S] cluster-binding residues, or that FeoCs lacking [Fe-S] cluster binding could be constitutively active and always capable of affecting iron transport.

To this end, we determined the NMR structure of *Vc*FeoC, which is generally similar to the previously solved *Ec* and *Kp*FeoC structures (Fig. 3 and Table 2). As expected, *Vc*FeoC features the conserved N-terminal, trihelical HTH domain but differs at the C-terminal winged  $\beta$ -sheet [10, 11]. Two main differences are observed between *Vc*FeoC and its [Fe-S] cluster-binding homologs: *Vc*FeoC features a shorter  $\beta$ -sheet and wing regions and has a long, disordered C-terminal tail (Fig. 3) [11]. In particular, we believe that the observed differences in

the winged  $\beta$ -sheet are due to differences in [Fe-S] cluster binding capabilities: *Ec*- and *Kp*FeoC bind [4Fe-4S] clusters requiring long, dynamic wings that undergo conformational changes to accommodate this cofactor [11, 16, 17], whereas *Vc*FeoC does not. We know that [Fe-S] cluster binding in *Ec*- and *Kp*FeoC results in compaction of structure [17], and we believe that *Vc*FeoC could naturally mimic this more compact structure without need of [Fe-S] cluster binding in order to affect function via protein-protein interactions.

FeoC is known to interact with other components of the Feo system, although a consensus on function still seems unclear. BACTH assays of the *V. cholerae* Feo system show that FeoB and FeoC interact [12], and immunoprecipitation studies demonstrate that FeoA, FeoB, and FeoC could form a complex, albeit very large [20]. Interestingly, this work proposed a requirement for FeoA but not FeoC in complex formation and suggested that FeoC could serve to regulate FeoB levels [20]. Moreover, the same assays implicated two *Vc*FeoC residues (Glu<sup>29</sup> and Met<sup>35</sup>) in giving rise to interactions with FeoB, but other participating residues were not identified. Our structural work demonstrates that the winged  $\beta$ -sheet of *Vc*FeoC binds full-length *Vc*FeoB with a modest  $K_d$  (*ca.* 25  $\mu$ M), and several residues including the previously proposed Glu<sup>29</sup>, but not Met<sup>35</sup>, are involved in *Vc*FeoB binding. Although the size of *Vc*FeoB prohibits the determination of the binding interface via NMR, docking studies suggest that the cavity formed by the GDI domain and the Switch I/II regions of *Vc*NFeoB acts as the binding receptacle for *Vc*FeoC. However, our data do not support the formation of a strong complex between only *Vc*FeoB and *Vc*FeoC, at least under these conditions. Considering the *in vivo* findings that FeoA, FeoB, and FeoC all interact in *V. cholerae* [20], it is plausible that the presence of *Vc*FeoA could strengthen the *Vc*FeoB-*Vc*FeoC interaction. In fact, this complex formation could even be nucleotide-mediated, and recent work from our lab has shown that FeoA-FeoB interactions can

be facilitated by the presence of nucleotide [38]. Ultimately, these events may be related to  $\text{Fe}^{2+}$  translocation via the transmembrane domain, especially given FeoC's interactions near the GDI domain that links directly to the first transmembrane helix. However, additional mechanistic and structural work is necessary to further probe this hypothesis, which is an exciting future avenue of research.

## Abbreviations

BACTH, bacterial adenylate cyclase two-hybrid; CV, column volume; DDM, n-dodecyl- $\beta$ -D-maltopyranoside; DtxR, diphtheria toxin repressor; *EcFeoC*, *Escherichia coli* FeoC; EDTA, ethylenediaminetetraacetic acid;  $\text{Fe}^{2+}$ , ferrous iron;  $\text{Fe}^{3+}$ , ferric iron; FNR, fumarate and nitrate reductase; GDI, GDP dissociation inhibitor; HSQC, heteronuclear single quantum coherence; IPTG, isopropyl- $\beta$ -D-1-thiogalactopyranoside;  $K_d$ , dissociation constant; *KpFeoC*, *Klebsiella pneumoniae* FeoC; LTTR, LysR transcriptional regulator; MWCO, molecular-weight cutoff; NMR, nuclear magnetic resonance; NOE, nuclear Overhauser effect; NOESY, nuclear Overhauser effect spectroscopy; PMSF, phenylmethylsulfonyl fluoride; RMSD, root-mean-square deviation; SH3, SRC homology 3; SEC, size exclusion chromatography; TEV, tobacco etch virus; *Vibrio cholerae* FeoB, *VcFeoB*; *Vibrio cholerae* FeoC, *VcFeoC*; *Vibrio cholerae* NFeoB, *VcNFeoB*; XNOE, heteronuclear nuclear Overhauser effect

## Acknowledgements

This work was supported by NSF CAREER grant 1844624 (A. T. S. and M. L.), NIH-NIGMS grant R35 GM133497 (A. T. S. and J. B. B.), and in part by NIH-NIGMS grant T32 GM066706 (M. L.). Sequence searches utilized both database and analysis functions of the Universal Protein Resource (UniProt) Knowledgebase and Reference Clusters (<http://www.uniprot.org>) and the National Center for Biotechnology Information (<http://www.ncbi.nlm.nih.gov/>). We thank Prof. Michael F. Summers (UMBC) for generous access to NMR facilities, reagents, and technical support.

## Statements and Declarations

### *Competing interests*

The authors declare no competing financial interest.

## References

- 1 K. D. Krewulak and H. J. Vogel (2008) *Biochim Biophys Acta* 1778:1781-1804
- 2 S. C. Andrews, A. K. Robinson and F. Rodríguez-Quinones (2003) *FEMS Microbiol Rev* 27:215-237
- 3 K. G. Wooldridge and P. H. Williams (1993) *FEMS Microbiol Rev* 12:325-348
- 4 E. P. Skaar (2010) *PLoS Pathog* 6:e1000949
- 5 J. B. Brown, M. A. Lee and A. T. Smith (2021) *Biochemistry* 60:3277-3291
- 6 M. Miethke and M. A. Marahiel (2007) *Microbiol Mol Biol Rev* 71:413-451
- 7 H. Contreras, N. Chim, A. Credali and C. W. Goulding (2014) *Curr Opin Chem Biol* 19:34-41
- 8 C. K. Lau, H. Ishida, Z. Liu and H. J. Vogel (2013) *Journal of Bacteriology* 195:46-55
- 9 E. T. Eng, A. R. Jalilian, K. A. Spasov and V. M. Unger (2008) *J Mol Biol* 375:1086-1097
- 10 K. W. Hung, J. Y. Tsai, T. H. Juan, Y. L. Hsu, C. D. Hsiao and T. H. Huang (2012) *J Bacteriol* 194:6518-6526
- 11 K. W. Hung, T. H. Juan, Y. L. Hsu and T. H. Huang (2012) *J Biomol NMR* 53:161-165
- 12 E. A. Weaver, E. E. Wyckoff, A. R. Mey, R. Morrison and S. M. Payne (2013) *J Bacteriol* 195:4826-4835
- 13 S. E. Maddocks and P. C. F. Oyston (2008) *Microbiology* 154:3609-3623
- 14 M. L. Cartron, S. Maddocks, P. Gillingham, C. J. Craven and S. C. Andrews (2006) *Biometals* 19:143-157
- 15 J. A. D'Aquino, J. Tetenbaum-Novatt, A. White, F. Berkovitch and D. Ringe (2005) *Proc Natl Acad Sci U S A* 102:18408-18413
- 16 K. L. Hsueh, L. K. Yu, Y. H. Chen, Y. H. Cheng, Y. C. Hsieh, S. C. Ke, K. W. Hung, C. J. Chen and T. H. Huang (2013) *J Bacteriol* 195:4726-4734
- 17 A. T. Smith, R. O. Linkous, N. J. Max, A. E. Sestok, V. A. Szalai and K. N. Chacón (2019) *Biochemistry* 58:4935-4949

- 18 J. C. Crack, M. R. Stapleton, J. Green, A. J. Thomson and N. E. Le Brun (2014) *Biochem J* 463:83-92
- 19 V. R. Sutton, E. L. Mettert, H. Beinert and P. J. Kiley (2004) *J Bacteriol* 186:8018-8025
- 20 B. Stevenson, E. E. Wyckoff and S. M. Payne (2016) *J Bacteriol* 198:1160-1170
- 21 A. E. Sestok, R. O. Linkous and A. T. Smith (2018) *Metallomics* 10:887-898
- 22 S. Grzesiek and A. Bax (1992) *J Am Chem Soc* 114:6291-6293
- 23 S. Grzesiek and A. Bax (1992) *J Magn Reson* 99:201-207
- 24 L. E. Kay, M. Ikura, R. Tschudin and A. Bax (1990) *J Magn Reson* 89:496-514
- 25 R. T. Clubb, V. Thanabal and G. Wagner (1992) *J Magn Reson* 97:213-217
- 26 F. Delaglio, S. Grzesiek, G. W. Vuister, G. Zhu, J. Pfeifer and A. Bax (1995) *J Biomol NMR* 6:277-293
- 27 M. Norris, B. Fetler, J. Marchant and B. A. Johnson (2016) *J Biomol NMR* 65:205-216
- 28 B. A. Johnson and R. A. Blevins (1994) *J Biomol NMR* 4:603-614
- 29 B. A. Johnson (2004) *Methods Mol Biol* 278:313-352
- 30 P. Güntert (2004) *Methods Mol Biol* 278:353-378
- 31 Y. Shen, F. Delaglio, G. Cornilescu and A. Bax (2009) *J Biomol NMR* 44:213-233
- 32 W. L. DeLano (2002),
- 33 M. Mirdita, K. Schütze, Y. Moriwaki, L. Heo, S. Ovchinnikov and M. Steinegger (2021) *BioRxiv*, doi <https://doi.org/10.1101/2021.08.15.456425>
- 34 J. Jumper, R. Evans, A. Pritzel, G. Tim, M. Figurnov, O. Ronneberger, K. Tunyasuvunakool, R. Bates, A. Zidek, A. Potapenko, A. Bridgland, C. Meyer, S. A. A. Kohl, A. J. Ballard, A. Cowie, B. Romera-Paredes, S. Nikolov, R. Jain, J. Adler, T. Back, S. Petersen, D. Reiman, E. Clancy, M. Zielinski, M. Steinegger, M. Pacholska, T. Berghammer, S. Bodenstein, D. Silver, O. Vinyals, A. W. Senior, K. Kavukcuoglu, P. Kohli and D. Hassabis (2021) *Nature* 596:583-589
- 35 D. Kozakov, D. R. Hall, B. Xia, K. A. Porter, D. Padhorny, C. Yueh, D. Beglov and S. Vajda (2017) *Nat Protoc* 12:255-278

- 36 D. Kozakov, D. Beglov, T. Bohnuud, S. E. Mottarella, B. Xia, D. R. Hall and S. Vajda (2013) Proteins: Struc, Funct, Bioinf 81:2159-2166
- 37 R. O. Linkous, A. E. Sestok and A. T. Smith (2019) Proteins 87:897-903
- 38 A. E. Sestok, J. B. Brown, J. O. Obi, S. M. O’Sullivan, E. D. Garcin, D. J. Deredge and A. T. Smith (2021) BioRxiv, doi <https://doi.org/10.1101/2021.09.29.462438>
- 39 V. Breukels, A. Konijnberg, S. M. Nabuurs, J. F. Doreleijers, N. V. Kovalevskaya and G. W. Vuister (2011) Current protocols in protein science. John Wiley & Sons, Inc, Hoboken, NJ, pp. 17.15.11-17.15.44
- 40 K. Wuthrich and G. Wagner (1979) J Mol Biol 130:1-18
- 41 D. S. Wishart and B. D. Sykes (1994) J Biomol NMR 4:171-180
- 42 A. M. Gronenborn and G. M. Clore (1994) J Biomol NMR 4:455-458
- 43 Y. Shen and A. Bax (2012) J Biomol NMR 52:211-232
- 44 L. Serrano and A. R. Fersht (1989) Nature 342
- 45 L. E. Kay, D. A. Torchia and A. Bax (1989) Biochemistry 28:8972-8979
- 46 L. E. Kay, G. M. Clore, A. Bax and A. M. Gronenborn (1990) Science 249:411-414
- 47 L. E. Kay, M. Ikura and A. Bax (1990) J Am Chemistry Soc 112:888-889
- 48 D. Marion, P. C. Driscoll, L. E. Kay, P. T. Wingfield, A. Bax, A. M. Gronenborn and G. M. Clore (1989) Biochemistry 28:6150-6156
- 49 G. W. Vuister, G. M. Clore, A. M. Gronenborn, R. Powers, D. S. Garrett, R. Tschudin and A. Bax (1993) J Magn Reson Series B 101:210-213
- 50 A. Ceccon, M. D’Onofrio, S. Zanzoni, D. L. Longo, S. Aime, H. Molinary and M. Assfalg (2013) Proteins 81:1776-1791
- 51 P. Y. Mercredi, N. Bucca, B. Loeliger, C. R. Gaines, M. Mehta, P. Bhargave, P. R. Tedbury, L. Charlier, N. Floquet, D. Muriaux, C. Favard, C. R. Sanders, E. O. Freed, J. Marchant and M. F. Summers (2016) J Mol Biol 428:1637-1655
- 52 H. Kim, H. Lee and D. Shin (2013) J Bacteriol 195:3364-3370

53 H. Kim, H. Lee and D. Shin (2015) J Bacteriol 197:92-98

For Table of Contents Use Only

# Ferrous iron transport protein C

